Journal of Materials Science: Materials in Electronics (2019) 30:11859–11867
https://doi.org/10.1007/s10854-019-01503-w

Structure and electrophysical properties of thin-film SnO_2–In_2O_3 heterostructures

O. V. Zhilova[1] · S. Yu. Pankov[1] · A. V. Sitnikov[1] · Yu. E. Kalinin[1] · M. N. Volochaev[2] · V. A. Makagonov[1]

Received: 30 January 2019 / Accepted: 13 May 2019 / Published online: 30 May 2019
© Springer Science+Business Media, LLC, part of Springer Nature 2019

Abstract

The structure and electrical properties of In_2O_3 and SnO_2 oxide semiconductors and heterostructures based on them has been experimentally investigated. The films were prepared by the method of layer-by-layer deposition using the ion-beam sputtering. The transition from the two-phase film of amorphous SnO_2 and In_2O_3 islands, formed during the layer-by-layer deposition, to a multilayer structure consisting of the amorphous SnO_2 and In_2O_3 continuous layers occurs with an increase in the bilayer thickness. The electrophysical properties of the $(SnO_2/In_2O_3)_{69}$ heterostructures are determined by the transition from the random distribution of SnO_2 and In_2O_3 amorphous phases to a multilayer structure and the temperature range of measurement. For all studied systems, a consistent change in the prevailing mechanism of conductivity is observed at temperatures from 77 to 300 K. In $(SnO_2/In_2O_3)_{69}$ thin films with a bilayer thickness $h_{bl} < 2.5$ nm, change of the prevailing conduction mechanism takes place according to the next sequence: variable range hopping conduction over localized states near the Fermi level, hopping conduction over the nearest neighbors and hopping transfer of carriers excited into localized states near the band edges at temperatures close to room temperature.

1 Introduction

Due to optical transparency and the possibility of changing the electrical conductivity in a wide range of values, wide-gap semiconductors based on metal oxides are subject to increased interest of researchers [1–3]. Already today such materials find application in various technical devices, for example, in flat-panel displays, solar cells, electrochromic devices, and many others [4–6]. In many cases the crystalline or amorphous structure of metal oxides mainly consists of metal cations and oxygen anions. As a result, the defects of the crystalline or amorphous structure are charged and electrically active, thereby exhibiting donor or acceptor properties [7]. It is assumed that bulk and surface defects in metal oxides significantly affect charge transfer and electrical conductivity. At the same time, the mechanisms of this influence remain largely unexplained.

✉ V. A. Makagonov
vlad_makagonov@mail.ru

[1] Voronezh State Technical University, Moskovskij Avenue, 14, Voronezh, Russia 394000

[2] Kirensky Institute of Physics FRC KSC SB RAS, Akademgorodok, 50, Krasnoyarsk, Russia 660036

Despite the great attention of the scientific community to the investigation of metal oxides, the nature of many experimentally observed features of optical, electrophysical, and galvanomagnetic properties remains unclear. This statement is especially true with respect to thin films, where the dimensionality of the system can play a significant role in addition to defects contribution. For example, in papers [8, 9] reported that the conditions of synthesis and subsequent heat treatment affect the electronic structure and optical properties of films.

The electrical conductivity of In_2O_3 and SnO_2 films substantially depends on the conditions of their synthesis [10, 11]. The values of electrical conductivity can be varied from typical for degenerate semiconductors with a band conduction mechanism to values characteristic for insulators with thermal activation or hopping conductivity. At a certain concentration of defects in metal oxide films the localization of charge carriers can occur. At the same time, the mechanisms of this localization and the parameters of localized electronic states remain poorly studied, while their understanding is important for obtaining films with high electron mobility and high transparency.

Currently, one of the most used metal oxide semiconductors is tin-doped indium oxide (ITO), which belongs to n-type degenerate semiconductors with a wide band gap

(3.6 eV) [12]. The density of conduction electrons in ITO thin films reaches 10^{19}–10^{21} cm^{-3}, and the mobility varies from 10 to 30 cm^2/V s [13]. ITO thin films can be prepared by various methods of synthesis, such as chemical vapor deposition, jet pyrolysis, DC or AC magnetron sputtering, pulsed laser deposition [14]. As in other semiconductor metal oxides, the electrical and optical properties of ITO thin films depend significantly on the structural state [15]. In this paper, we consider an experimental study the structure and its effect on the electrical properties of multilayer heterogeneous films of the In_2O_3–SnO_2 system obtained by layer-by-layer deposition at the ion-beam sputtering of ceramic targets of In_2O_3 and SnO_2 in an argon atmosphere to produce films with higher electron mobility and high optical transparency.

1.1 Samples and experimental technique

Thin films $(SnO_2/In_2O_3)_{69}$ were obtained by the ion beam sputtering of ceramic targets In_2O_3 and SnO_2 in an argon atmosphere with a purity of 99.998% at a pressure of 7×10^{-4} Torr according to the method described in [16]. The targets were fixed on water-cooled copper bases of 280×80 mm^2 in sizes and placed in different sputtering positions in a vacuum chamber. In order to carry out layer-by-layer deposition, the substrate was moved from one sputtering position to another by rotating the substrate holder around the axis of the sputtering chamber. The deposition was carried out on monocrystalline silicon substrates with a crystallographic orientation (100) for the study of the structure and on the sitall substrates for the study of electrophysical properties. In the process of deposition, the room temperature of the substrates was maintained [17]. To obtain different thicknesses of the In_2O_3 and SnO_2 layers in the course of a single deposition process, V-shaped screens were installed between the targets and the substrate holder.

To estimate the thickness of the layers, a preliminary deposition of individual In_2O_3 and SnO_2 films was carried out with process parameters previously selected for the deposition of a multilayer structure. The thickness of the obtained films was measured using the MII-4 optical interferometer. The measurement points for thickness were fixed relative to the location of the substrate and the target. The film thickness obtained during a single passage of the substrate through sputtering position (monolayer thickness of one of the deposited oxides) was calculated by dividing the resulting film thickness on the number of the substrate holder revolutions. The thickness of the second phase monolayer was determined in a similar way. It should be noted that the monolayer thickness obtained by this way is equivalent and does not take into account the possibility of island growth, i.e. this is the thickness of the thin film deposited in one revolution of the substrate holder, provided that this film is continuous.

The number of substrate holder revolutions determined the number of bilayers in a multilayer film $(SnO_2/In_2O_3)_{69}$, where 69 is the number of bilayers obtained by described method. The thicknesses of the layers In_2O_3 and SnO_2 varied from ~ 0.8 to ~ 2.1 nm and from ~ 0.4 to ~ 2.8 nm, respectively. The thickness of the bilayer at the same time varied from 1.2 to 4.9 nm.

The structure was studied by X-ray diffraction methods on a Bruker D2 Phaser diffractometer ($\lambda_{CuK\alpha1} = 1.54$ Å) using the software DIFFRAC.EVA 3.0 with the ICDD PDF Release 2012 database [17]. Transmission electron microscopy (TEM) studies were carried out using a Hitachi HT7700 TEM (acceleration voltage 100 kV, W source). The cross-sectional samples on the sitall substrates for TEM studies were prepared by focused ion beam (single-beam FIB, Hitachi FB2100) at 40 kV to a thickness of about 40–50 nm. In order to protect the surface from milling by the Ga+ ion beam during sample preparation, a Ge layer was deposited onto $(SnO_2/In_2O_3)_{69}$ film before cross-sectional sample preparation by FIB.

The dependences of the electrical resistivity on the thickness were measured by the two-probe method in DC mode using a B7-78/1 universal digital multimeter. The dependences of the thermopower on temperature were obtained by the differential method. The material of the cold and hot probes was silver wire with a purity of 99.99%. The relative error in measuring the electrical resistance did not exceed 2%, and the thermopower—3% [17].

The Hall effect measurements were carried out according to the Van-der-Pau method on square-shaped samples with a side of 8 mm on ECOPIA HMS-5500 apparatus at room temperature. Electrical contacts in the form of small indium points were made by ultrasonic soldering. The magnetic field with a magnetic flux density of 0.55 T was created by permanent magnets, and a measuring current was 0.1–2.0 mA, depending on the sample response.

1.2 Film structure

An analysis of the X-ray diffraction patterns for In_2O_3 and SnO_2 thin films showed that SnO_2 films are amorphous and In_2O_3 films are nanocrystalline (Fig. 1). The calculation of the average crystallite size for In_2O_3 films was performed according to the Scherrer formula [18, 19]

$$D = \frac{0.89\lambda}{b\ \cos\Theta}, \tag{1}$$

where λ is the x-ray wavelength (1.54 Å for $Cu_{K\alpha}$ radiation); b is the reflex width at half-height; Θ is the Bragg angle; D is the average size of the crystallites. The estimates for In_2O_3 films gave D ≈ 20 nm.

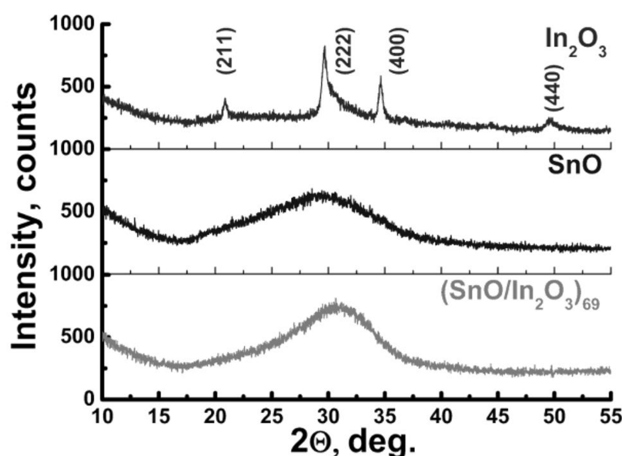

Fig. 1 X-ray diffraction patterns for SnO and In_2O_3 thin films and $(SnO/In_2O_3)_{69}$ layered heterostructures

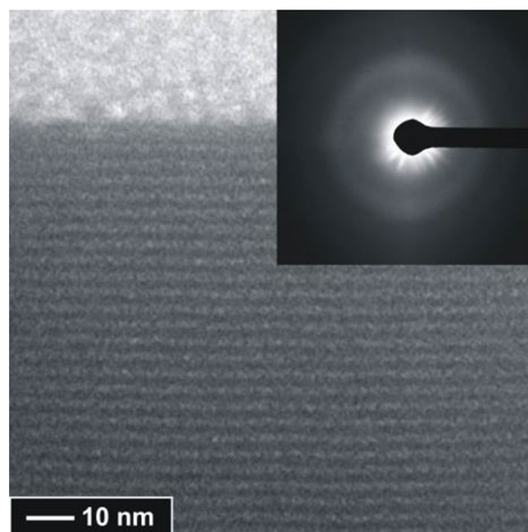

Fig. 2 TEM micrographs of the cross section and electron diffraction pattern (inset) for $(SnO/In_2O_3)_{69}$ thin films with equivalent bilayer thickness $h_{bl} = 2.61$ nm

In the X-ray diffraction pattern for $(SnO_2/In_2O_3)_{69}$ thin films at $2\Theta = 10–60°$ there is one broad maximum (halo) (Fig. 1). The diffraction maximum at $2\Theta \approx 30.7°$ does not depend on the film thickness (layer thickness), and the position and shape of the peak coincide well with the diffraction pattern for the amorphous SnO_2 film and with the most intense diffraction peak of the cubic In_2O_3. Thus the layers of In_2O_3 and SnO as part of multilayer system $(SnO_2/In_2O_3)_{69}$ have an X-ray amorphous structure, whereas the structure of separately deposited indium oxide thin films is nanocrystalline.

For a more detailed analysis of the structure of $(SnO_2/In_2O_3)_{69}$ thin films, the cross section investigation was carried out using transmission electron microscopy (TEM) (Fig. 2). An analysis of TEM micrographs confirmed the formation of a layered structure in the $(SnO_2/In_2O_3)_{69}$ films. The presence of two wide halos and the absence of diffraction rings from the crystal planes in the electron diffraction pattern of the $(SnO_2/In_2O_3)_{69}$ films confirm the conclusion that the structure of the SnO_2 and In_2O_3 interlayers is amorphous (Fig. 2).

The formation of a multilayer structure from amorphous SnO_2 and In_2O_3 layers may indicate insolubility or rather low solubility of tin and indium oxides in each other at layer-by-layer deposition condition at room temperature. The In_2O_3 layers as part a multilayer system $(SnO_2/In_2O_3)_{69}$ are amorphous whereas for a separate synthesized thin film of indium oxide the structure is crystalline.

1.3 Experimental results

Figure 3 shows the dependences of the specific electrical resistance ρ and thermopower S versus equivalent bilayer thickness, measured for layered thin-film heterostructures of $(SnO_2/In_2O_3)_{69}$ (Fig. 3a, b, respectively).

With an increase in the equivalent bilayer thickness to $h_{bl} \sim 2.8$ nm, a decrease in the electrical resistivity (ρ) and thermopower (S) of layered thin-film heterostructures is observed. Such decreasing in the electrical resistance was observed in other thin films systems [20] and usually associated with the transition from island layers to formation of a layered structure $(SnO_2/In_2O_3)_{69}$ with continuous SnO_2 and In_2O_3 interlayers. The sign of the thermopower for all investigated films is negative, which indicates that the main charge carriers in both SnO_2 and In_2O_3 thin films and in layered $(SnO_2/In_2O_3)_{69}$ thin-film heterostructures are electrons.

In order to estimate the effect of the concentration and mobility of charge carriers on the specific electrical resistance, the Hall effect in layered thin-film heterostructures of $(SnO_2/In_2O_3)_{69}$ was studied. The results of these studies showed that the dependences between the concentration n and the mobility μ_e of free charge carriers and the equivalent bilayer thickness for layered thin-film heterostructures $(SnO_2/In_2O_3)_{69}$ have a complex shape (Fig. 4). The concentration of charge carriers is $n \sim 10^{20}$ cm^{-3}, it increases several times with a thickness corresponding to the transition from an island structure to a multilayer one. The obtained values are consistent with the results of In_2O_3 thin films study [21]. The charge carriers' mobility slightly decreases until $h_{bl} < 2.5$ nm, and then increases by an order of magnitude with increasing $h_{bl} > 2.5$ nm.

To explain the observed data, it is necessary to return to the process of growth of layered thin-film heterostructures on a rotating substrate during ion-beam sputtering of SnO_2 and In_2O_3 targets. At the $h_{bl} < 2.5$ nm, the $(SnO_2/In_2O_3)_{69}$ film is the island interlayers that is equivalent to the formation of a two-phase amorphous system. The electrical

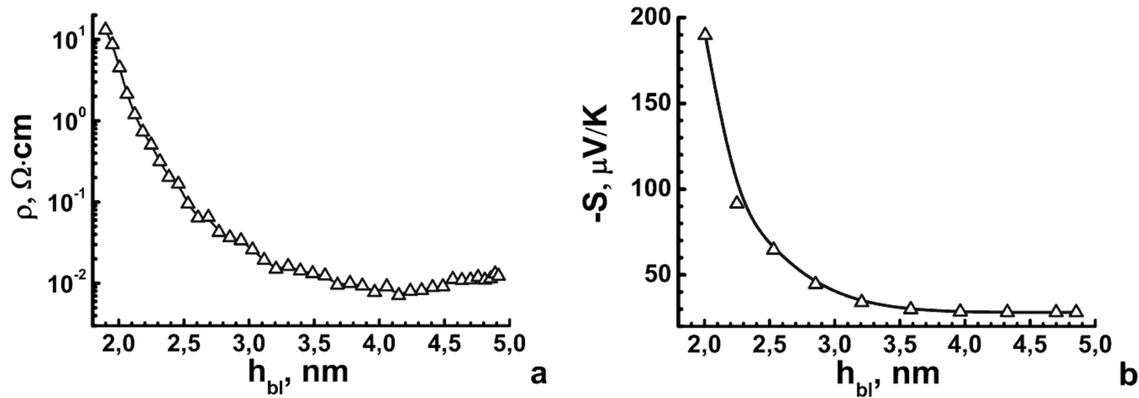

Fig. 3 Dependences of the electrical resistivity (**a**) and thermopower (**b**) versus equivalent bilayer thickness h_{bl} of $(SnO_2/In_2O_3)_{69}$ layered thin-film heterostructures

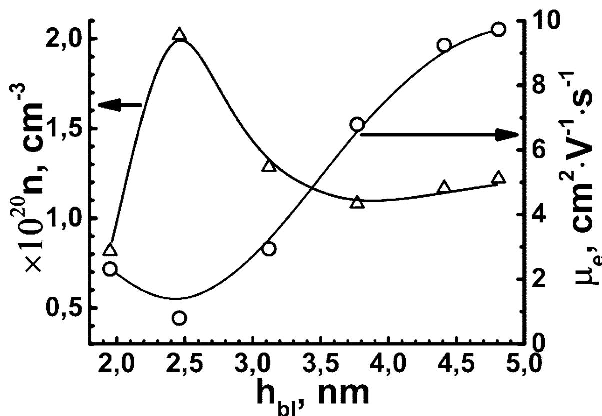

Fig. 4 Dependences of the concentration n and the mobility μ_e of free charge carriers versus the equivalent bilayer thickness (h_{bl}) for $(SnO_2/In_2O_3)_{69}$ layered thin-film heterostructures

conductivity of such system is determined by the ratio of the most conductive In_2O_3 and the least conductive SnO_2 oxide phases. With an increase in the size of indium oxide islands in interlayers, they contact with each other and form a quasi-two-dimensional percolation cluster. This increases the concentration of dangling bonds at the interfaces, and, therefore, electrons (Fig. 4). As a result the electrical resistivity of the film is reduced (Fig. 3a). An increase in the defectiveness of the transfer channel (the main source of charge carriers in wide-gap semiconductors is oxygen vacancies) reduces the electron mobility due to their localization (Fig. 4). This also leads to a blurring of the localized states band and decrease in the derivative of the density of electronic states of dn/dE. As a result, the thermoelectric power decreases (Fig. 3b). In other words, the presence of a chaotic potential due to randomly distributed charges in the space charge region at the interfaces of a semiconductor multilayer structure leads to strong localization [22].

At $h_{bl} > 2.5$ nm, a layered structure is formed from amorphous SnO_2 and In_2O_3 continues interlayers. In this case, it can be assumed that In_2O_3 interlayers will be the main conduction channel. As the thickness of the In_2O_3 interlayers increases, there will be a transition from strong localization to the so-called weak localization state [23, 24]. This leads to an increase in carrier mobility (Fig. 4).

To establish the dominant mechanisms of electrical transfer in the obtained multilayer systems, the temperature dependences of the electrical resistivity ρ(T) and the thermopower S(T) were studied in the temperature range from 80 to 300 K (Fig. 5). As can be seen in Fig. 5a, as the temperature increases, the electrical resistance of the studied samples decreases, and the thermopower curve has a maximum (Fig. 5b).

1.4 Discussion of the results

The observed experimental results are discussed taking into account the peculiarities of the $(SnO_2/In_2O_3)_{69}$ heterostructures growth process upon layer-by-layer deposition of SnO_2 and In_2O_3. At the $h_{bl} < 2.5$ nm the film is characterized by an island structure, which is equivalent to the formation of a two-phase amorphous system. The electrical conductivity of such systems is determined by the ratio of the most conductive In_2O_3 phase and the least conductive phase of SnO_2. Let us consider the features of the electric transfer processes based on the analysis of the temperature dependences of the specific electrical resistance and thermopower of such heterogeneous systems.

For the $(SnO_2/In_2O_3)_{69}$ films with $h_{bl} < 2.5$ nm the obtained experimental dependences of the electrical resistance on temperature (Fig. 5a) were replotted in the coordinates lnR vs $1/T^n$, where n took values ¼, ½, 1, lnR versus lnT and lnR versus ln (1/T). The dependencies of the thermopower (Fig. 5b) were represented in the coordinates S versus lnT, S versus 1/T and S

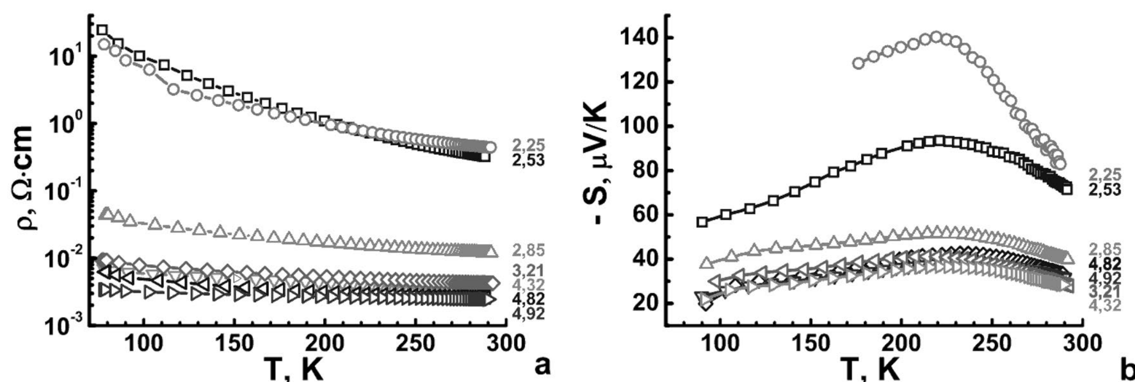

Fig. 5 Dependences of the electrical resistance (**a**) and thermopower (**b**) versus temperature for $(SnO_2/In_2O_3)_{69}$ layered thin-film heterostructures. The thickness of the bilayer h_{bl} in nm is indicated near the curves

versus $1/T^{1/2}$ [17]. Joint analysis of the depicted on Fig. 5 data showed that at temperatures of 80–180 K the electrical resistivity and thermopower are linear in the coordinates lnR versus $1/T^{1/4}$ and S versus $1/T^{1/2}$ (Fig. 6). According to the model of hopping conductivity with variable jump length over localized states lying in a narrow energy band near the Fermi level [25], the expression for electrical conductivity is as follows [17]

$$\sigma = e^2 \cdot \mathrm{R}^2 \cdot \nu_{\mathrm{ph}} \cdot g \cdot \exp\left(-\frac{\mathrm{B}}{\mathrm{T}}\right)^{1/4}, \tag{2}$$

where

$$\mathrm{B} = \frac{16}{\mathrm{a}^3 \cdot \mathrm{k} \cdot g(\mathrm{E_F})} \tag{3}$$

and

$$\mathrm{R} = \left[\frac{3}{2\pi \cdot \mathrm{a} \cdot g(\mathrm{E_F}) \cdot \mathrm{k} \cdot \mathrm{T}}\right]^{1/4}, \tag{4}$$

E is the electron charge, R is the hopping length, v_{ph} is the factor of the phonon–phonon interaction, T is the absolute temperature, $g(E_F)$ is the density of states at the Fermi level, a is the localization radius of the electron wave function, k is the Boltzmann constant.

The values of B in Eq. 2 for the studied films were determined from Fig. 6a. Assuming that the process of carrier transport is limited by jumps between indium dangling bonds, to estimate the density of localized states, we take the localization radius equal to the radius of the ion In a ≈ 1 nm [26]. Then, according to [17], applying expressions (2)–(4), it is possible to estimate the parameters of an amorphous multilayer film using the hopping electron conductivity model with variable jump length over localized states lying in a narrow energy band near the Fermi level (Table 1).

The average jump energy has been estimated also (Table 1), which in the case of variable-jump lengths should be equal to [25]

$$\mathrm{W_{VRH}} \cong \mathrm{k}\left(\mathrm{BT^3}\right)^{1/4}. \tag{5}$$

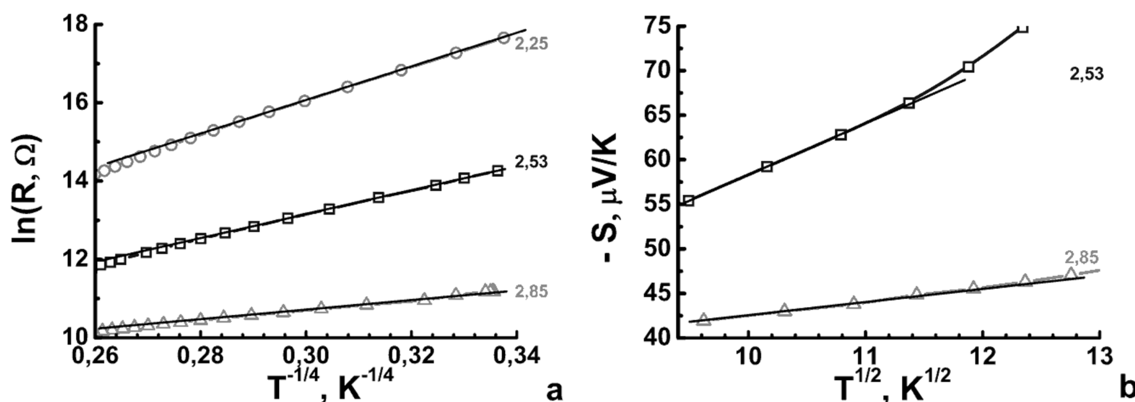

Fig. 6 Dependences of lnR versus $1/T^{1/4}$ (**a**) and S versus $1/T^{1/2}$ (**b**) for thin films $(SnO_2/In_2O_3)_{69}$. The thickness of the bilayer h_{bl} in nm is indicated near the curves

Table 1 Parameters of $(SnO_2/In_2O_3)_{69}$ thin films, calculated in frames of the electron hopping model with variable jump length over localized states lying in a narrow energy band near the Fermi level, in the temperature range 80–180 K

h_{bl}, nm	$B^{1/4}$	B, K	$g(E_F)$,1/(eV cm^3)	R at 180 K, nm	S, μV/K (T = 180 K)	$\left(\frac{\partial \ln g(E)}{\partial E}\right)_{E=E_F}$ eV^{-1} (T = 180 K)	W_{VRH}, eV (T = 180 K)
2.25	40.86	2.79×10^6	6.66×10^{19}	4.64			0.173
2.53	39.83	2.52×10^6	7.38×10^{19}	4.52	85.02	7.90×10^{-6}	0.169
2.85	13.05	29×10^3	6.40×10^{21}	1.48	48.52	2.25×10^{-6}	0.055

If the hopping mechanism of conduction with a variable hopping length is due to localized states lying in a narrow energy band near the Fermi level in the studied temperature range is dominant, then the thermopower should be written as [25]

$$S = \frac{k^2}{2e}\sqrt{T \cdot B}\left(\frac{\partial \ln g(E)}{\partial E}\right)_{E=E_F}. \quad (6)$$

The experimental values of the thermopower in the temperature range of 80-190 K, where the Mott law is true for electrical conductivity, satisfy the law $S \sim f\ (1/T^{1/2})$ (Fig. 6b). Taking into account the previously obtained values of B from the temperature dependences lnR versus $1/T^{1/4}$ and experimental data S (Fig. 6b), it is possible to estimate the logarithm of the density of localized states with respect to energy for different temperatures [25]. The results of such estimates for the $(SnO_2/In_2O_3)_{69}$ films studied at T = 180 K are presented in Table 1.

To describe the temperature dependences of electrical conductivity in the temperature range of 180–250 K, we apply the model of hopping conductivity over nearest neighbors; then, according to [25], for the electrical resistivity and thermoelectric power

$$\rho = \rho_1 \cdot \exp\left(-\frac{W_{NNH}}{kT}\right), \quad (7)$$

and

$$S = \frac{2\pi}{3}\frac{k^2 T}{e}\left(\frac{\partial \ln g(E_F)}{\partial E}\right)_{E=E_F}, \quad (8)$$

where W_{NNH} is the activation energy of the jump, given for jumping over the nearest neighbors by the expression [17]

$$W_{NNH} = \frac{3}{4\pi R_0^3 g(E_F)}, \quad (9)$$

where R_0 is the average distance between the nearest neighbors, $g(E_F)$ is the density of states at the Fermi level.

The experimental dependences of the electrical resistance and thermopower in the temperature range of 180–250 K have linear dependences in the coordinates lnR versus 1000/T and S versus T, respectively (Fig. 7a, b). Using formulas (7) and (8), we estimate from Fig. 7a, b the values of the jump activation energy and the derivatives of the logarithm of the density of localized states. The results are shown in Table 2.

In the temperature range 250–300 K, the dependences of the electrical resistivity and thermopower have linear segments in the coordinates lnR versus 1000/T and S versus 1000/T (Fig. 8a, b, respectively). Then, the following

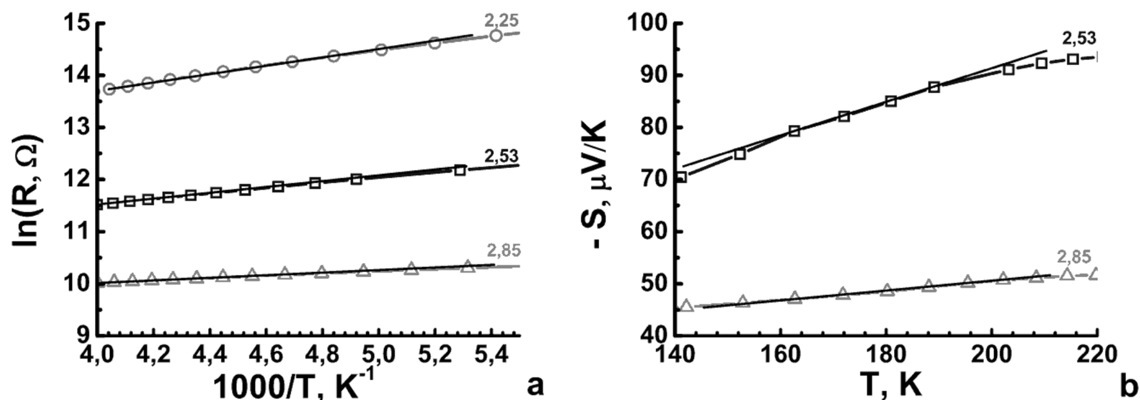

Fig. 7 Dependences of lnR versus 1000/T (**a**) and S versus T (**b**) for thin films $(SnO_2/In_2O_3)_{69}$. The thickness of the bilayer h_{bl} in nm is indicated near the curves

Table 2 Parameters of $(SnO_2/In_2O_3)_{69}$ thin films, calculated from the model of the hopping conductivity of electrons over the nearest neighbors

h_{bl}, nm	S, μV/K (T = 190 K)	$\left(\frac{\partial \ln g(E)}{\partial E}\right)_{E=E_F}$ eV^{-1} (T = 190 K)	W_{NNH}, eV	R_0, nm (T = 190 K)
2.25	40.86	2.79×10^6	–	–
2.53	39.83	2.52×10^6	0.035	0.22
2.85	13.05	29×10^3	0.015	0.73

Table 3 Activation energies of conduction and thermopower, as well as the average jump energy for $(SnO_2/In_2O_3)_{69}$ thin films in the temperature range of 250–300 K

h_{bl}, nm	E_a^R, eV	E_a^S, eV	W_h, eV
2.25	0.077 ± 0.005	0.077 ± 0.005	
2.53	0.042 ± 0.005	0.036 ± 0.005	0.006 ± 0.001
2.85	0.02 ± 0.005	0.019 ± 0.005	0.001 ± 0.0005

equations are valid for the temperature dependences of the thermopower and electrical resistivity [17]

$$\rho = \rho_0 \cdot \exp\left(-\frac{E_a^R}{2kT}\right), \tag{10}$$

where E_a^R is the activation energy of electrical conductivity. k is the Boltzmann constant, T is the absolute temperature.

$$S = \pm\frac{k}{e}\cdot\left(\frac{E_a^S}{kT} + A\right), \tag{11}$$

where e is the electron charge, A is the constant, E_a^S is the activation energy of the thermopower. Taking into account Eqs. (10) and (11), the experimental dependences (Fig. 8a, b) can be used to estimate the values of the activation energy of the conductivity E_a^R and the thermoelectric power E_a^S. The results of this assessment are shown in Table 3.

An analysis of the experimental results (Table 3) showed that the calculated values of the activation energy of electrical conductivity and thermopower within the error limit coincide only for the bilayer thickness $h_{bl} = 2.25$ nm. In this case, we can talk about the hopping mechanism by the nearest neighbors in the tail of the conduction band. For large thicknesses of the bilayer, the values of the activation energy of electrical conductivity and thermopower differ by a certain quantity W_h, which increases with decreasing thickness of the bilayer. If we take the hopping mechanism as the conduction mechanism in the studied composites, then, according to [25], the difference in the energies of E_a^R and E_a^S can act as a criterion for determining the hopping conductivity with a variable jump length for localized states in the tail of the conduction band. Then the energy W_h can be interpreted as the energy of the jump, and formula (10) will be more correctly rewritten in the form [17]

$$\rho = \rho_0 \cdot \exp\left(-\frac{E_a^{R*} + W_h}{2kT}\right), \tag{12}$$

where $E_a^{R*} = E_a^S = E_A - E_F$, E_A is the energy at the edge of the conduction band, E_F is the Fermi, energy E_a^{R*} is the activation energy of electrical conductivity, k is the Boltzmann constant, T is the absolute temperature.

The experimental dependences of the electrical resistance on temperature (Fig. 5a) for films with $h_{bl} > 2.8$ nm are satisfactorily straightened in the coordinates ρ versus lnT (Fig. 9). These dependences are typical for 2D and 3D systems where conditions of weak localization of electrons

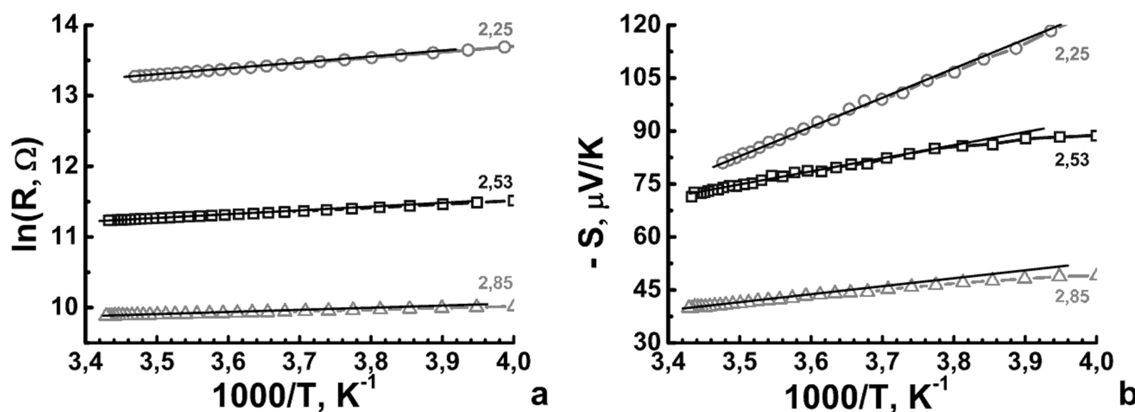

Fig. 8 Dependences lnR versus 1000/T (**a**) and S versus 1000/T (**b**) for thin films $(SnO_2/In_2O_3)_{69}$. The thickness of the bilayer h_{bl} in nm is indicated near the curves

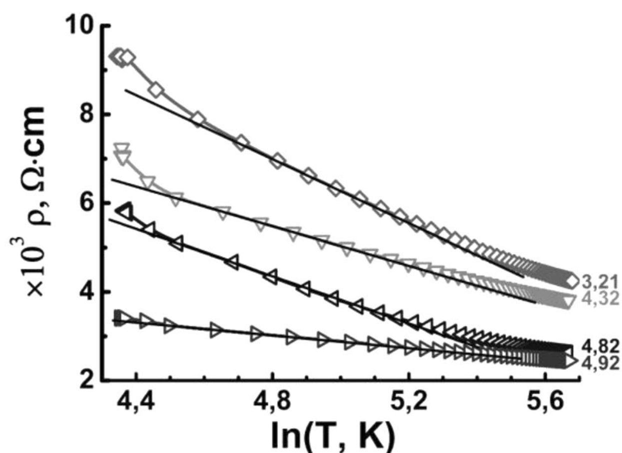

Fig. 9 Dependences ρh vs lnT for thin films of $(SnO_2/In_2O_3)_{69}$. The thickness of the bilayer h_{bl} in nm is indicated near the curves

are realized and the theory of quantum corrections to conductivity is applicable [23].

Similar temperature dependences of the resistance was observed in In_2O_3:Sn films with a thickness of 7.5–1980 nm which was accompanied by negative magnetoresistance [27, 28]. This phenomenon was described by the authors in the framework of the theory of quantum corrections to conductivity in the weak localization mode for 2D and 3D systems. Temperature dependences of electrical resistance showed a minimum characteristic of weak localization. The minimum of electrical resistance temperature shifts toward lower temperatures with increasing film thickness. The indium oxide layers in the present work have a lower interlayer thickness, therefore, the minimum of electrical resistance in the studied temperature range is not observed. However, with an increase in the thickness of indium oxide layers, the deviation temperature from the linear depence ρ versus lnT shifts toward lower temperatures with an increase in the thickness of the interlayer. Further research in this direction will confirm or refute the hypothesis put forward.

2 Conclusion

During the layer-by-layer deposition by the ion-beam sputtering, heterogeneous $(SnO_2/In_2O_3)_{69}$ thin films are formed. The $(SnO_2/In_2O_3)_{69}$ films has a rather complex structure, which depends on the thickness of the bilayer. At $h_{bl} < 2.5$ nm, $(SnO_2/In_2O_3)_{69}$ films consist of amorphous island SnO_2 and In_2O_3. With an increase in the equivalent thickness of more than 2.5 nm, continuous amorphous In_2O_3 and SnO_2 layers form a multilayer structure.

The structure of the $(SnO_2/In_2O_3)_{69}$ films and the temperature range of their study determine their electrophysical properties. It has been established that for thin films of $(SnO_2/In_2O_3)_{69}$ with $h_{bl} < 2.5$ nm, there is a consistent change of the prevailing conduction mechanism: a variable range hopping conduction over localized states near the Fermi level, hopping conduction over the nearest neighbors and hopping transfer of carriers excited into localized states near the band edges at close to room temperatures.

Acknowledgements The authors of the article want to express their gratitude to Professor S.A. Gridnev for helpful discussions. This work was supported by the Ministry of Education and Science in the framework of the state task (project No: 3.1867.2017/4.6).

Compliance with ethical standards

Conflict of interest The authors declare that they have no conflict of interest.

References

1. SZh Karazhanov, Phase Stability, electronic structure, and optical properties of indium oxide polytypes. Phys. Rev. B **76**(7), 075129 (2007)
2. J.E. Medvedeva, D.B. Buchholz, R.P.H. Chang, Recent advances in understanding the structure and properties of amorphous oxide semiconductors. Adv. Electron. Mater. **3**(9), 1700082 (2017)
3. M.A. Korotin, Magnetic state of iron impurity ions in In_2O_3. JETP Lett. **108**(8), 537–542 (2018)
4. C.G. Granqvist, *Handbook of Inorganic Electrochromic Materials* (Elsevier Science, Amsterdam, 1995)
5. O.N. Mryasov, A.J. Freeman, Electronic band structure of indium tin oxide and criteria for transparent conducting behavior. Phys. Rev. B **64**(23), 233111 (2001)
6. A.J. Freeman, Chemical and thin-film strategies for new transparent conducting oxides. MRS Bull. **25**(8), 45–51 (2000)
7. M.M. Mezdrogina, Parameters of ZnO films with p-type conductivity deposited by high-frequency magnetron sputtering. Semiconductors **51**(5), 559–564 (2017)
8. V.F. Agekyan, Formation of Cu_2O and ZnO crystal layers by magnetron assisted sputtering and their optical characterization. Semiconductors **52**(3), 383–389 (2018)
9. A.A. Tikhii, Influence of the thermal conditions of fabrication and treatment on the optical properties of In_2O_3 films. Semiconductors **52**(3), 320–323 (2018)
10. M. Maache, T. Devers, A. Chala, Al-doped and pure ZnO thin films elaborated by sol-gel spin coating process for optoelectronic applications. Phys. Technol. Semicond. **51**(12), 1663–1668 (2017)
11. YuE Kalinin, Effect of heat treatment on the electrical properties of thin yttrium-doped In_2O_3 films. Inorg. Mater. **54**(9), 885–891 (2018)
12. C.G. Granqvist, A. Hultaker, Transparent and conducting ITO films: new developments and applications. Thin Solid Films **411**(1), 1–5 (2002)
13. A. Ambrosini, Electrical, optical, and structural properties of tin-doped In_2O_3–M_2O_3 solid solutions (M=Y, Sc). J. Solid State Chem. **153**(1), 41–47 (2000)
14. S.D. Ginley, H. Hosono, D.C. Paine, *Handbook of Transparent Conductors* (Springer, New York, 2011)
15. B. Buchholz, The structure and properties of amorphous indium oxide. Chem. Mater. **26**(18), 5401–5411 (2014)

16. V.V. Rylkov, Tunneling anomalous hall effect in nanogranular CoFe–B–Al–O films near the metal-insulator transition. Phys. Rev. B **95**(14), 144202 (2017)
17. YuE Kalinin, Properties of amorphous carbon thin films grown by ion beam sputtering. Tech. Phys. **62**(11), 1724–1730 (2017)
18. M. Maddahfar, M. Ramezani, S.M. Hosseinpour-Mashkani, Barium hexaferrite/graphene oxide: controlled synthesis and characterization and investigation of its magnetic properties. Appl. Phys. A **122**(8), 752 (2016)
19. A. Javidan, M. Ramezani, A. Sobhani-Nasab, S.M. Hosseinpour-Mashkani, Synthesis, characterization, and magnetic property of monoferrite $BaFe_2O_4$ nanoparticles with aid of a novel precursor. J. Mater. Sci. **26**(6), 3813–3818 (2015)
20. V.V. Balashev, Electrical and magnetic properties of ultrathin polycrystalline Fe films grown on SiO_2/Si (001). Tech. Phys. Lett. **44**(7), 595–598 (2018)
21. V.G. Kytin, Conducting properties of In_2O_3: Sn thin films at low temperatures. Appl. Phys. A **114**(3), 957–964 (2013)
22. V.B. Bondarenko, A.V. Filimonov, Criterion for strong localization on a semiconductor surface in the Thomas–Fermi approximation. Semiconductors **51**(10), 1321–1325 (2017)
23. T.A. Polyanskaya, YuV Shmartsev, Quantum correction to the conductivity of semiconductor with a two-dimensional and a 3-dimensional electron-gas. Exp. Sov. Phys. Semicond.-USSR **23**(1), 1–19 (1989)
24. M. Nistor, F. Gherendi, J. Perrière, Degenerate and non-degenerate In_2O_3 thin films by pulsed electron beam deposition. Mater. Sci. Semicond. Process. **88**, 45–50 (2018)
25. N. Mott, E. Davis, *Electronic Processes in Non-Crystalline Materials* (Clarendon Press, Oxford, 1979)
26. G.V. Samsonov, *Handbook of the Physicochemical Properties of the Elements* (Springer, New York, 1968)
27. T. Ohyama, M. Okamoto, E. Otsuka, Weak localization and correlation effects in indium-tin-oxide films. II. Two-to-three dimensional transition and competition between localization and superconductivity. J. Phys. Soc. Jpn. **54**(3), 1041–1053 (1985)
28. T. Ohyama, M. Okamoto, E. Otsuka, Weak localization and correlation effects of two dimensional electrons in indium-tin-oxide films. J. Phys. Soc. Jpn. **52**(10), 3571–3578 (1983)

Publisher's Note Springer Nature remains neutral with regard to jurisdictional claims in published maps and institutional affiliations.